Journal of Building Engineering 70 (2023) 106373

Contents lists available at ScienceDirect

Journal of Building Engineering

journal homepage: www.elsevier.com/locate/jobe

Photocatalysis of functionalised 3D printed cementitious materials

Behzad Zahabizadeh [a,*], Iran Rocha Segundo [b,c,**], João Pereira [a,d], Elisabete Freitas [b], Aires Camões [e], Vasco Teixeira [c], Manuel F.M. Costa [f], Vítor M.C.F. Cunha [a], Joaquim O. Carneiro [c]

[a] ISISE, Institute of Science and Innovation for Bio-Sustainability (IB-S), Department of Civil Engineering, University of Minho, 4800-058, Guimarães, Portugal
[b] ISISE, Department of Civil Engineering, University of Minho, 4800-058, Guimarães, Portugal
[c] Centre of Physics of Minho and Porto Universities (CF-UM-UP), University of Minho, Azurém Campus, 4800-058, Guimarães, Portugal
[d] Innovation Point, Rua de Pitancinhos – Palmeira, 4700-727, Braga, Portugal
[e] University of Minho, CTAC, Department of Civil Engineering, 4800-058, Guimarães, Portugal
[f] Centre of Physics of Minho and Porto Universities (CF-UM-UP), University of Minho, Gualtar Campus, 4704-553, Braga, Portugal

ARTICLE INFO

Keywords:
3D concrete printing
TiO_2 nanoparticles
Photocatalytic behaviour
Surface roughness
Smart functionalised composite

ABSTRACT

The main objective of this study was to evaluate the photocatalytic behaviour of 3D printed cementitious mortars that were functionalised with TiO_2 nanoparticles. This study is one of the few available regarding functionalisation of 3D concrete printing (3DCP) with photocatalytic properties. Despite the fact 3DCP research is swiftly growing, it is still necessary further investigation to fully understand these materials' physicochemical and mechanical properties, which will influence the functionalised properties of the composite. Due to the freeform nature of the 3DCP there are no moulds, therefore the functionalisation through coating can be performed in a much earlier stage than in conventional moulded concrete. The developed smart 3D printed concrete could promote the photodegradation of pollutants for self-cleaning and air purification. In particular, this study investigated the effect of two parameters on photocatalytic behaviour: light power intensity and the coating rate of nano-TiO_2 particles. Surface coating was adopted as the functionalisation method, and the Rhodamine B dye degradation efficiency was used as an indicator to evaluate the photocatalytic behaviour. Additionally, the surface roughness and microstructure of the 3D printed cementitious mortar specimens were assessed to distinguish between the reference and TiO_2 coated series. Scanning electron microscopy (SEM), X-ray Energy-dispersive spectroscopy (EDS), and X-ray diffraction (XRD) crystallography were carried out as three techniques to evaluate the morphology, composition, and microstructure of the specimens, respectively. The results indicated successful activation of catalyst particles under illumination, where higher light power intensity increased the degradation efficiency. Furthermore, dye degradation efficiency increased with increasing coating rates of nano-TiO_2 particles on the surface of the specimens. The roughness of the 3D printed specimens' surface was sufficient for

* Corresponding author.
** Corresponding author. ISISE, Department of Civil Engineering, University of Minho, 4800-058, Guimarães, Portugal.
E-mail addresses: b.zahabizadeh@civil.uminho.pt (B. Zahabizadeh), iran@civil.uminho.pt (I. Rocha Segundo), joaodaniel.pereira@innovpoint.com (J. Pereira), efreitas@civil.uminho.pt (E. Freitas), aires@civil.uminho.pt (A. Camões), vasco@fisica.uminho.pt (V. Teixeira), mfcosta@fisica.uminho.pt (M.F.M. Costa), vcunha@civil.uminho.pt (V.M.C.F. Cunha), carneiro@fisica.uminho.pt (J.O. Carneiro).

https://doi.org/10.1016/j.jobe.2023.106373
Received 13 October 2022; Received in revised form 3 March 2023; Accepted 23 March 2023
Available online 25 March 2023

settling the nano-TiO_2 particles. Finally, microscopy results confirmed the presence and suitable distribution of the nano-TiO_2 particles on the surface of the coated specimens.

1. Introduction

In the last decades, the increase of environmental pollutants has become one of the major concerns worldwide, since it is directly or indirectly related to population health issues [1–3]. Air pollutants, such as ground level ozone, carbon monoxide, and nitrogen oxides (NO_x), among others, released due to the gas emission from the industrial activities and traffic exhausts, may cause several types of illnesses, such as respiratory and lung diseases, which can significantly influence the quality of life of an human beings [4–8]. Moreover, polluted urban areas and soot fouling are two reasons for the life cycle reduction of construction materials that may deteriorate the aesthetic performances of the built environments' surfaces [9,10]. Since construction materials cover an extensive area of the build environment, adding the photocatalytic function to such materials is one of the methods for improving the quality of the environment through organic pollutants degradation, self-cleaning, self-sterilisation, air and water purification and solar energy conversion, among others [6–8,11,12]. Reduction in the maintenance efforts and costs of cleaning the surface of buildings/infrastructures is another advantage of adding photocatalytic functionalisation to the construction materials [13].

Photocatalytic materials using semiconductors are capable of photodegrading organic and inorganic pollutants [14,15]. Electron-hole pairs are generated with the incidence of a photon with a higher energy than the band gap of the semiconductor, which react with humidity and oxygen producing species with a high ability of oxidation and reduction [16]. High chemical stability, high oxidising and reducing ability, non-toxicity, and lower price of TiO_2 particles make them the most employed semiconductors for these purposes when compared to other compounds [1,13,17–19].

TiO_2 is found on three crystalline phases: anatase, rutile, and brookite [8,12]. Anatase can demonstrate the highest photocatalytic activity due to its higher exposed structure compared to the other two mineral forms of TiO_2 [20,21]. The higher exposed surface area of anatase can enhance the hydroxylation degree of the adsorbing surface, and consequently decrease the velocity of electron-hole pairs recombination [8]. Nonetheless, it is reported that combining anatase and rutile, can improve the efficiency of photocatalytic behaviour compared to the individual application of each crystalline phase [22]. The photocatalytic efficiency of TiO_2 can be influenced by the number of crystalline phases, particle size, specific surface area, exposed surface facets, pore volume and the structure of

Table 1
Definition of the specimens' series, the type of test performed, and related sections of the results.

Specimens' Series	TiO_2 Coating Rates [mg/cm^2]	Type of Tests/Related Sections of Results				
		Surface Roughness	Photocatalytic Efficiency	Microstructure's Analysis		
				SEM	EDS	XRD
Ref	-[a]	✓[g] Sec. 3.1	✓ Sec. 3.2.3	✓ Sec. 4.1	✓ Sec. 4.2	✓[f] Sec. 4.3
CR5	5	✓ Sec. 3.1	✓ Sec. 3.2.3	✓ Sec. 4.1	✓ Sec. 4.2	-
CR10	10	-	✓ Sec. 3.2.3	-	-	-
CR20	20	-	✓ Sec. 3.2.3	✓ Sec. 4.1	✓ Sec. 4.2	-
CR40	40	-	✓ Sec. 3.2.3	-	-	-
CR80	80	✓ Sec. 3.1	✓ Sec. 3.2.3	✓ Sec. 4.1	✓ Sec. 4.2	✓[f] Sec. 4.3
CR10 (L)[b]	10	-	✓ Sec. 3.2.2	-	-	-
CR10 (D)[c]	10	-	✓ Sec. 3.2.2	-	-	-
CR20 (L)[b]	20	-	✓ Sec. 3.2.2	-	-	-
CR20 (D)[c]	20	-	✓ Sec. 3.2.2	-	-	-
CR20 (LPI 1 mW/cm^2)[d]	20	-	✓ Sec. 3.2.1	-	-	-
CR20 (LPI 8 mW/cm^2)[e]	20	-	✓ Sec. 3.2.1	-	-	-

Notes:
[a] Ref considered as non-coated series.
[b] CR10 (L) & CR20 (L) tested under **L**ight irradiation.
[c] CR10 (D) & CR20 (D) were tested under **D**arkness.
[d] CR20 was tested under irradiation with **L**ight **P**ower **I**ntensity of **1 mW/cm^2**.
[e] CR20 was tested under irradiation with **L**ight **P**ower **I**ntensity of **8 mW/cm^2**.
[f] XRD test was carried out on **Top** surface and **C**ross **S**ection of series Ref and CR80 designated as $Ref_{(TOP)}$, … $Ref_{(CS)}$, $CR80_{(TOP)}$, and $CR80_{(CS)}$, respectively in Sec. 4.3.
[g] The check mark symbols show the type of tests performed on the specimens' series.

TiO_2 particles [23,24].

Cementitious construction materials with a porous structure, strong binding ability and the existence of compatibility between their alkaline nature and semiconductors are defined as an ideal medium for applying the semiconductors' particles, in particular TiO_2 [6,18,19,25–27]. Different methods, such as surface coating and volume incorporation are used to apply TiO_2 particles in cementitious materials [6,8,13,19,23,28–30].

The main novelty related to this work is the fact that it is one of the few (as far as the authors are aware) that studies the influence of surface morphology (surface roughness) and microstructure of 3D printed cementitious mortars (which is different from conventional cementitious mortars) on their photocatalytic properties resulting from the inclusion of nanoparticles of semiconductor materials (titanium dioxide). Moreover, it also studies the influence of light power intensity and the coating rate of nano-TiO_2 particles on the photocatalytic efficiency of 3D printed cementitious mortars. Regarding the photocatalysis, the focus was on the RhB dye degradation efficiency as an indicator of the self-cleaning performance. The combination of photocatalysis and 3DCP can result in an improved product as a multifunctional cementitious mortar. Even though the number of research works is growing fast in the field of 3DCP in both cases of process and material characterisation, still in-depth research is necessary regarding functionalisation of these materials. Therefore, in this study a 3DCP is combined with photocatalysis through a surface coating approach to produce a smart multifunctional cementitious material in an automated fashion.

2. Materials and experimental methods

This section discusses the materials and functionalisation method, followed by an explanation of different test methods on the functionalised samples. Table 1 shows the definition of the specimens' series, the type of test performed, and related sections of the results.

2.1. Materials

2.1.1. Cementitious mixture

Cement CEM I 42.5 R, fly ash type F and silica fume were used as binders in the mortar composition. The other constituents comprised fine quartz sand with a maximum aggregate size of 1 mm, a polycarboxylate based superplasticiser and water. A water to binder ratio (W/B) of 0.31 was adopted. The partial replacement of cement by additions, such as fly ash and silica fume, i.e., two by-products, can reduce the usage of Portland cement and therefore contribute to decreasing the ecological footprint [31], as well as contribute to the densification of the matrix and hence having stiffer matrix [32], while maintaining adequate fresh properties [33]. Table 2 includes the mortar composition per cubic meter and specific mass of its constituents, while Table 3 resumes the main mechanical and physical properties at the curing age of 28 days. A comprehensive description of the development process and characterisation of the mechanical properties of this composition can be found elsewhere [33,34].

2.1.2. Semiconductor

TiO_2 nanoparticles (nano-TiO_2) were used as the semiconductor catalysts to endow photocatalytic functionality to the developed 3D printed cementitious specimens. The nano-TiO_2 consisted of 80% anatase, and 20% rutile and were acquired from Quimidroga Company, Spain. The band gap energy of the nano-TiO_2 was measured through a diffuse reflectance device and calculated based on the Kubelka-Munk theory [35]. The results showed an energy band gap equal to 3.19 eV for the nano-TiO_2 particles used in this study.

2.1.3. Nano-TiO_2 aqueous suspension

Three different concentrations of the nano-TiO_2 aqueous suspensions were prepared, including 4, 8 and 16 g/L. The nano-TiO_2 particles have a high tendency to agglomerate due to their large surface area to volume ratio [8]. Therefore, a pH of 8 was adopted for all the suspensions to reduce their tendency to agglomerate and consequently have more stable colloidal suspension [13]. In fact, the negative value of the zeta potential for the nano-TiO_2 dispersion at the pH of 8 [13] can improve the nano-TiO_2 dispersion quality through the formation of the Coulomb forces. Although, it is reported that a lower pH can enhance the oxidising activity of TiO_2, at the same time, the acidic condition can reduce the specific surface area of the semiconductor due to the enhancement of the agglomeration tendency of the particles [11]. Moreover, using a suspension with a pH of 8 could also reduce the risk of any negative effect on the properties of the cementitious materials with alkaline nature.

2.2. Sample preparation and functionalisation

In this study, semiconductor particles were coated on a cementitious matrix for 3DCP developed in a previous experimental work [33,34]. Fig. 1 shows the process of preparation and functionalisation of the cementitious mortar specimens. A small 3D concrete

Table 2
Ternary mortar composition.

Material	Quantity [kg/m^3]	Specific mass [g/cm^3]
Sand	1183.0	2.66
Cement	286.0	3.11
Fly ash	423.0	2.35
Silica fume	79.0	2.25
Water	248.0	1.00
Superplasticizer	10.2	1.04

Table 3
Mechanical/physical properties of the cementitious mortar composition at the curing age of 28 days.

Specific weight [g/cm^3]		Porosity [%]		Elasticity modulus E_c [GPa]			Compressive strength f_{cm} [MPa]			Flexural strength $f_{cf,fe}$ [MPa]		
PS[a]	MC[b]	PS	MC	PS		MC	PS		MC	PS		MC
				L-Pa[c]	L-Pe[d]		L-Pa	L-Pe		L-Pa	L-Pe	
2.16	2.15	11.3	–	33.9	27.2	36.4	51.0	50.2	58.0	6.8	6.8	6.6

[a] Printed Specimens.
[b] Mould Cast.
[c] Loaded Parallel to the layers' orientation.
[d] Loaded Perpendicular to the layers' orientation.

printer was used to create the cementitious mortar specimens (Fig. 1a). The detailed information about the 3D concrete printer can be found elsewhere [33]. In this experimental work, specifically for printing the specimens for photocatalytic tests, a custom-made rectangular nozzle in PLA was designed and printed using a commercial 3D printer. The extrusion dimensions of the nozzle were 25 × 9.5 mm^2 (Fig. 1a). Several cementitious mortar batches were prepared, and the 3D printed elements comprised just two layers with the dimensions of 250 × 25 × 15 mm^3, see Fig. 1 b. The height of each layer was set at 7.5 mm to have the final height of 15 mm for each printed strip. Finally, the printed strips were cut immediately after printing to prepare the final specimens with adequate dimensions (i.e., 25 × 25 × 15 mm^3) for the photocatalytic tests (Fig. 1c). This method was used to eliminate any post-treatment process of the specimens at later ages, such as using conventional cutting hardware for hardened concrete. Since these conventional methods usually use water during cutting, dust and cement paste originated during the cutting could cover the surface of specimens resulting in covering the semiconductors' particles and ultimately biasing the photocatalytic results.

In this work, the surface coating methodology was selected to functionalised the 3D printed cementitious specimens based on previous research studies from the authors on asphalt and cementitious materials [13,15,36,37]. In this method, an atmospheric air compressor (Fig. 1d) was used to spray the nano-TiO_2 aqueous suspension onto the surface of specimens. The freeform capabilities of 3DCP technology allowed spraying the TiO_2 particles on the surface of the elements immediately at the end of the printing process, when the cementitious material was still fresh. Spraying the semiconductors in the fresh state of cementitious materials could improve the immobilization of the TiO_2 particles, i.e., the bond quality between the particles and the specimens. The application of this coating method has already been used for conventional mould cast concrete, however note that the semiconductor particles can only be sprayed after removing the moulds, therefore after the concrete has hardened, which may affect the adherence of the semiconductor particles to the surface. Additionally, the smoother surface of the cast elements, due to the mould boundary conditions, may also contribute to decrease the bond of the semiconductor particles and consequently reduce the photocatalytic efficiency. This removal of the semiconductor particles from the surface may be more prone when under environmental conditions, such as by e.g., wind and rain [22,38]. A detailed description of this coating method can be found in Ref. [15]. Various coating rates in the range from 5 mg/cm^2 to 80 mg/cm^2 onto the surface of specimens could be obtained through the coating method based on the given volumes of the nano-TiO_2 aqueous suspension.

Considering the applied technique for functionalisation of the samples, it should be mention that the surface coating technique is the most efficient and easiest functionalisation method compared to other methodologies, such as volume incorporation [3,8,13,17,

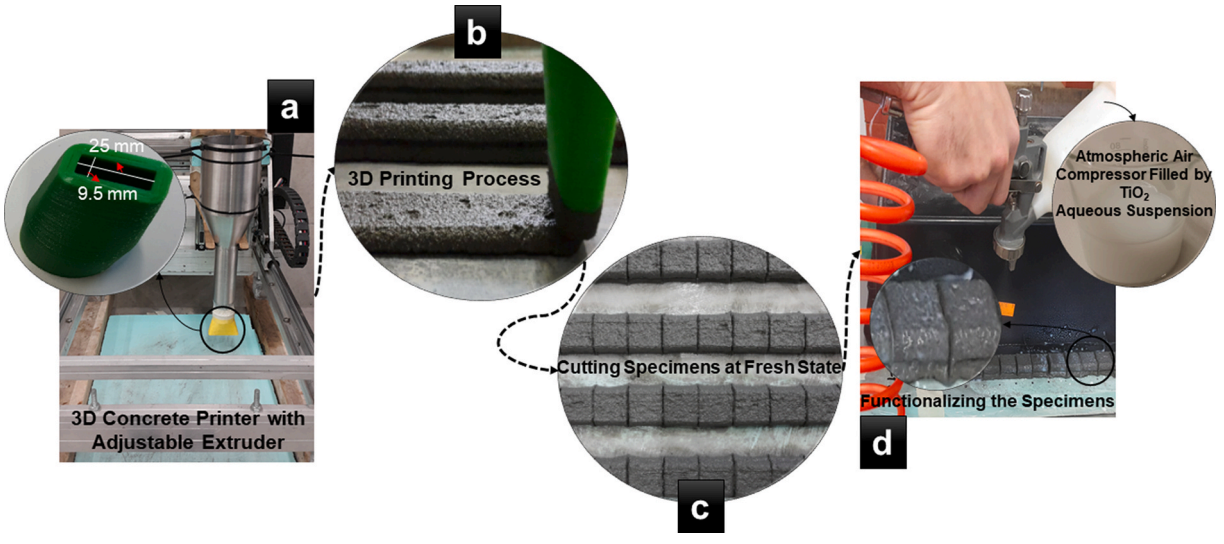

Fig. 1. Preparation and functionalisation of the cementitious specimens.

39]. In the coating technique, a higher number of semiconductor particles are exposed to light on the surface when compared to the volume incorporation method [9]. Therefore, photocatalytic activity can be enhanced by increasing the number of semiconductor particles exposed to light irradiation [8,9,13]. Some studies revealed that even by adding high amounts of TiO_2 powder in the bulk of cementitious mixtures, the specimens showed lower photocatalytic efficiency than the samples coated by spraying the semiconductor suspension [8,13,17]. Therefore, higher amounts of semiconductors must be used to have the same distribution of the TiO_2 particles on the surface when they are added to the mixture [8,9]. On the other hand, using the TiO_2 particles as volume incorporation may influence the rheological and mechanical properties of the material [6,8,22,30,40,41] that can be an obstacle when using some of the new construction technologies such as 3D concrete printing (3DCP).

2.3. Test procedures

2.3.1. Surface roughness of 3D printed cementitious mortars

The micro-analysis was carried out to evaluate the surface roughness of the printed specimens. For the micro-surface analysis, the MICROTOP.06.MFC device was used as a non-destructive and non-contact method. This technology is a versatile and robust system that is mainly designed for 2D/3D micro-topographic analysis of the rough surfaces of small size samples [42]. The MICROTOP.06.MFC setup has an active optical triangulation system in which the scanning of the sample's surface is carried out through an oblique incidence of a light beam and a normal/specular observation [42,43]. Fig. 2 shows a general perspective of the setup. Additional information regarding the setup, including the definitions of each component, as well as a detailed description of the scanning mechanism, can be found elsewhere [42,43]. In this study, 701 × 201 points in an area of 4 × 4 mm^2 were scanned on the surface of the specimens. The reference specimen (Ref) and two TiO_2 coated specimens, namely, one with the lowest coating rate (CR5, i.e., 5 mg/cm^2) and other with the highest coating rate (CR80, i.e., 80 mg/cm^2) were selected to evaluate their surface roughness.

Several important surface roughness parameters were calculated to infer the surface characterisation of the 3D printed specimens. The main studied roughness parameters include average roughness (S_a), Root-Mean-Square deviation (S_q), total roughness height (S_t), maximum peak height (S_p), maximum valley depth (S_v), space between the peaks or irregularities (S_m), skewness (S_{sk}), kurtosis (S_{ku}), area of the peak portion (S_{r1}), and area of the valley portion (S_{r2}). A detailed description and illustration of these parameters and the method of calculations can be found in Refs. [44–46].

2.3.2. Photocatalytic efficiency

Generally, two different approaches are used to measure the degradation of organic compounds, such as Rhodamine B (RhB). The

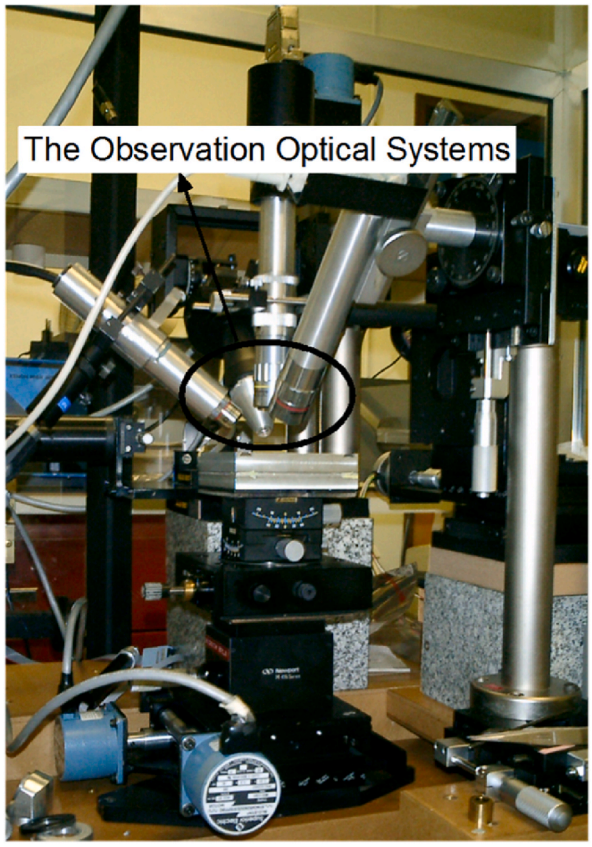

Fig. 2. General perspective of the MICROTOP.06.MFC setup.

first approach is based on coating the surface of the samples with a specific amount of dye solution and make a visual and semi-qualitative assessment of the dye colour variation under light irradiation [6,39], or by a more accurate method such as reflectance spectroscopy [23,25,26,28]. In the second approach, the samples are immersed in a dye solution and the degradation of dye is measured through the evaluation of the solution decolouration using absorbance spectroscopy [7,13,47]. The main limitation of the first approach is its dependency on the colour of the samples. Measuring the dye colour variation is impractical when the dye solution is dried on the surface of the dark colour materials such as compositions containing fly ash or calcium aluminate [26]. However, this limitation does not exist for the second approach since it was used successfully even for asphalt materials with black surface colour [7, 13,36]. Additionally, this method is simple, using mainly a conventional UV–Vis spectrophotometer and a light source. Therefore, in this study the second approach was carried out to evaluate the photocatalytic efficiency.

The photocatalytic activity of the functionalised cementitious specimens was evaluated based on their capability in the dye degradation efficiency as a model. Rhodamine B (RhB) was used as an organic cationic dye compound. In general, the RhB model has been commonly used as an organic pollutant to assess the effectiveness of treatment methods and develop strategies to mitigate environmental pollution, considering its application on a wide range of substances such as textiles [48], papers [49], polymers [12], construction materials [22], etc. The RhB compound, with quite low sensitivity to the alkaline nature of the cementitious materials [6, 23], was used in the form of an aqueous solution with a concentration of 5 mg/L (5 ppm). The RhB degradation rate in the aqueous solution was measured based on the maximum absorbance of the light at a wavelength of 554 nm. Fig. 3 shows the process for measuring the dye degradation efficiency. All the samples were immersed in 30 mL of the RhB aqueous solution for 3 h under dark conditions (Fig. 3a and c). Then, the immersed specimens were irradiated by a 300 W OSRAM UltraVitalux lamp (Fig. 3d) to simulate the solar irradiation. At the centre of the photocatalytic box and a constant vertical distance of 25 cm between the top surface of the specimens and the source of light, the irradiation power intensity of 8 mW/cm^2 was measured through a Quantum Photo Radiometer HD9021 Delta Padova. During the test process under light irradiation, the system containing the RhB solution and the immersed specimen was covered by a transparent plastic film (Fig. 3b). The plastic film was used to prevent the evaporation of RhB aqueous solution due to produced heat by the lamp. This plastic film could transmit at least 90% of the light rays in the range of wavelength between 292 and 900 nm, so it had a negligible effect on the light quality received by the specimens [7].

The specimens were irradiated for a maximum period of 20 h. At 1, 2, 4, 8 and 20 h of light exposure, an aliquot of 3 mL RhB aqueous solution was picked up from the each system (Fig. 3e) to measure its light absorbance in the wavelength ranges of 300–800 nm using a Shimadzu UV-2501 PC spectrophotometer (Fig. 3f). Afterwards, the photocatalytic efficiency was calculated based on the maximum absorbance value at the wavelength of 554 nm (Fig. 3g) using the Beer-Lambert law [7,13,50] according to Equation (1):

$$\boldsymbol{\Phi}(t)\ [\%] = ((\boldsymbol{A_0} - \boldsymbol{A}(t))\,/\,\boldsymbol{A_0}) \times 100 \tag{1}$$

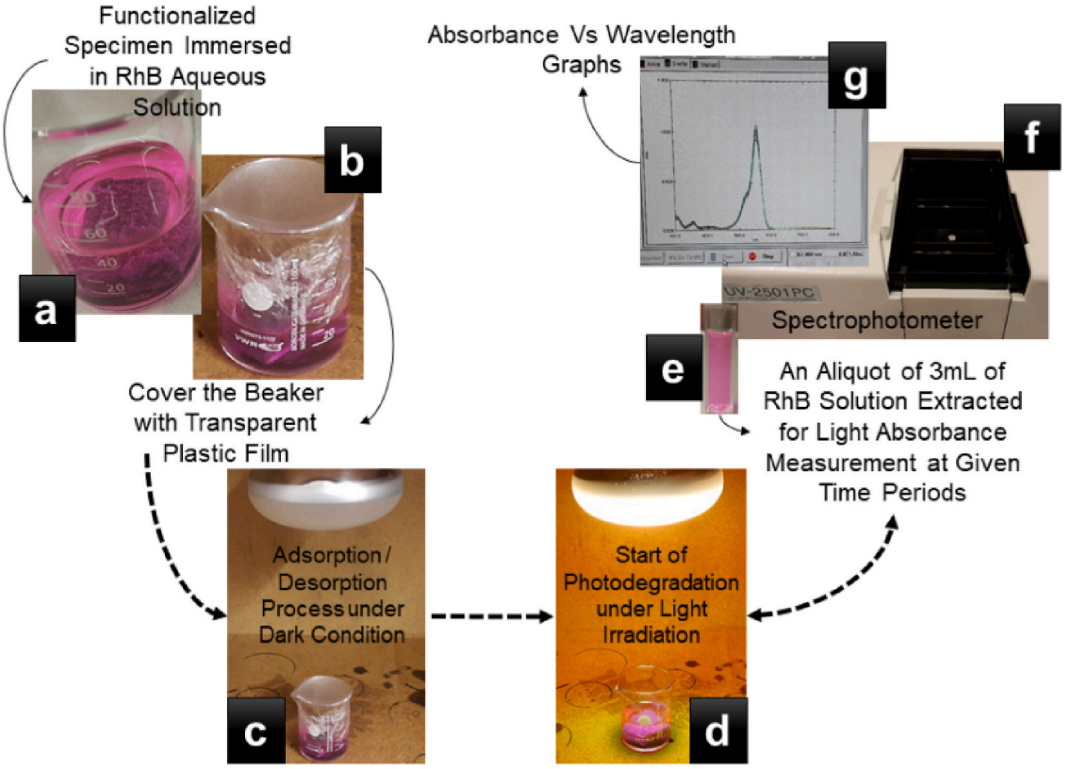

Fig. 3. The process of dye degradation efficiency measurement of the specimens.

where $\Phi(t)$ is the photocatalytic efficiency for time t [%]; A_0 and $A(t)$ are the maximum light absorbance of the RhB aqueous solution at time zero and t, respectively. The zero time was defined as the starting time of light irradiation (end of the dark condition), when the specimens reach the equilibrium of adsorption/desorption.

2.3.3. Microstructural, chemical and crystallography analysis

Concerning the microstructure analysis of the specimens, this study considered three different materials characterization techniques, namely the Scanning Electron Microscopy (SEM), Energy-dispersive X-ray spectroscopy (EDS) and X-Ray diffraction (XRD) analysis. These methods were utilized to assess the specimens' morphology, chemical composition, and microstructure, focusing on comparing the characteristics of non-coated and TiO_2-coated series. The advantages of these characterization techniques were to evaluate the distribution of nano-TiO_2 particles on the surface of the coated specimens considering their connection to other hydration products of cementitious material. Moreover, evaluation of the specimens' cross-section could reveal the potential penetration of the TiO_2 particles beneath the surface, considering the fresh state of the samples during the coating process. Using these characterization techniques could render a better understanding and inference of the results of photocatalytic efficiency.

2.3.3.1. Preparation of the specimens. In order to perform the microstructural analysis (Scanning electron microscopy - SEM), the surface of specimens was covered with a very thin film (20 nm) of Au–Pd (80-20 wt %). The covering process of the surface was carried out using a high-resolution sputter coater, 208HR Cressington Company, coupled to a MTM-20 Cressington High-Resolution Thickness Controller.

2.3.3.2. Scanning electron microscopy. The SEM, considering the morphological analysis of the specimens, was carried out through an Ultra-high resolution Field Emission Gun Scanning Electron Microscopy (FEG-SEM), NOVA 200 NanoSEM, FEI Company. Moreover, secondary electron images were taken at an acceleration voltage of 10 kV and atomic contrast images were realised with a Back-scattering Electron Detector (BSED) at an acceleration voltage of 15 kV. SEM was performed to evaluate the surface morphology of the specimens. Moreover, the dispersion of nano-TiO_2 particles and their arrangement considering the cementitious materials hydration products could be qualitatively assessed using SEM.

2.3.3.3. X-ray energy-dispersive spectroscopy. Chemical composition analyses of the samples were performed with the X-ray Energy Dispersive Spectroscopy (EDS) technique, using an EDAX Si(Li) detector at an acceleration voltage of 15 kV. EDS was performed to compare the chemical compounds present at the surface of the coated and uncoated (Ref) specimens. The cross section of the samples underneath the coated surface was also evaluated through EDS analysis.

2.3.3.4. X-ray diffraction crystallography. The minerals' crystal structure on the specimens' surface was analysed through the X-ray diffraction (XRD) technique, using the Bruker AXS D8 Discover diffractometer with Cu-Kα radiation ($\lambda = 1.54060$ Å). The analyses were carried out in the geometry configuration $\theta/2\theta$, at room temperature, by scanning between 10° and 85°, with a 0.02° step and integration time of 1 s per step. XRD analysis was carried out on the surface and along the cross section of the coated and uncoated (Ref) samples to compare the crystallographic structure of the material.

3. Photocatalytic analysis

3.1. Surface roughness

The surface roughness was assessed for 3D printed specimens from three distinct series, i.e., Ref, CR5 and CR80 corresponding to the uncoated specimens, TiO_2 surface coated with coating rates of 5 mg/cm^2 and 80 mg/cm^2, respectively. Fig. 4 shows a 3D illustration of the surface roughness of the specimen with the minimum TiO_2 coating rate (CR5) adopted in the present study.

In general, the surface roughness of 3D printed cementitious materials is higher than the one observed for cast concrete or mortar due to the absence of the mould's walls. In this study, the surface roughness of the mould cast mortar was not assessed since from a visual inspection there were clear differences between 3D printed and mould cast specimens. On the other hand, rough surfaces have a larger area and a significant part is less exposed to rain (for example, the recesses that can also accommodate and retain more nanoparticles), thus minimizing the probability of nanoparticles being removed from the material and therefore contributing to achieve better photocatalytic efficiency (which should also be maintained for longer periods of time). This aspect may contribute to a better settling of the nanoparticles on the surface of 3DCP and consequently lead to a higher durability of the functionalised coating.

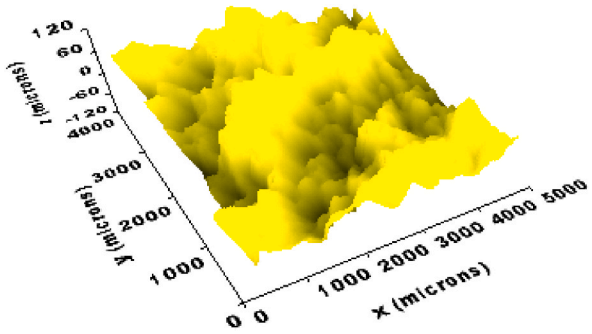

Fig. 4. 3D illustration for the surface roughness of the specimen with the minimum nano-TiO_2 coating rate of 5 mg/cm^2 (CR5).

The surface roughness assessment was carried out based upon the geometrical features of the top surfaces of the specimens, namely on the spacing, height, depth and area portions of the valleys and peaks obtained from 2D and 3D parameters of the surface profiles. In each series, the average results of two samples were reported.

Fig. 5a shows the arithmetic mean deviation, also known as average roughness (S_a), as well as the Root-Mean-Square deviation (S_q) of the surfaces. The average roughness and the Root-Mean-Square roughness both showed almost similar texture morphology for the surface of the specimens, with a maximum difference of less than 33% between Ref and CR5 series. However, other roughness parameters need also to be evaluated, in order to have a more comprehensive information about the conditions and distribution of the valleys and peaks on the surface [51,52]. It should be noticed that different surface profiles can show similar average roughness [51]. Therefore, other roughness parameters, such as the maximum total height (S_t), also known as the total roughness height, the maximum peak height (S_p) and the maximum valley depth (S_v) were evaluated to compare the surface texture of the specimens in more detail.

Fig. 5b shows S_t, S_p and S_v of the studied surfaces. The reference specimen (Ref) showed the highest total height and valley depth than the TiO_2 coated series (CR5 and CR80). The lower values for the total height and the valley depth in the TiO_2 coated specimens can be due to the distribution and accumulation of the semiconductor particles inside the valleys, resulting in reducing the valleys' depth. On the other hand, the maximum peak height was increased in both TiO_2 coated specimens compared to the reference one, which can also be due to the accumulation of the TiO_2 particles on the peaks of the surface. The specimen CR5 showed a higher peak height than valley depth but with a difference of about 2.5%.

Regarding the existing spaces between the peaks or irregularities (S_m), the results were more similar for TiO_2 coated series (CR5 and CR80), see Fig. 5c. However, the minimum spacing between the irregularities was observed on the reference specimens. By distributing the TiO_2 particles, some of the valleys could be filled and reach the height of smaller peaks, resulting in larger spaces between the irregularities for the TiO_2 coated series.

A negative skewness (S_{sk}) value obtained for all the series indicated the higher amounts of the valleys distributed on the topography of the scanned surfaces (i.e. a negative texture) [52], see Fig. 5d. In this case, the reference specimen showed the highest skewness resulting from the lack of symmetry in the height distribution that agrees with the results of valleys' depth. Nonetheless, regarding the TiO_2 coated series, the skewness values were quite small, near to zero, which showed irregularities on the specimens' surface were distributed more symmetrically when compared to the reference specimen. The governing of valleys on roughness profile can be due to the existence of deep holes or cracks on the surface [52]. Moreover, the valleys can be formed due to the printing process during the extrusion of the layers of the reference specimen, which then were filled by nano-TiO_2 particles in the coated series. Therefore, in the TiO_2 coated series, the skewness has decreased to nearly zero. On the other hand, the kurtosis (S_{ku}) was significantly higher than 3 for the reference specimens, which demonstrated the higher weight of the tails distribution (i.e. steep or sharp tails of valleys and peaks) in

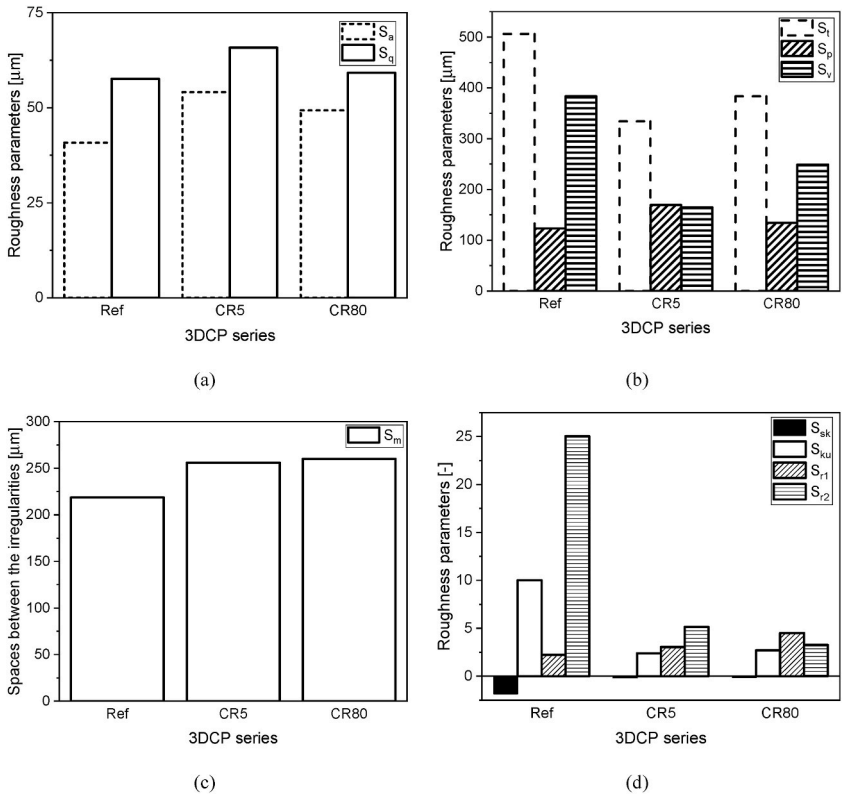

Fig. 5. Surface roughness parameters for the 3D printed cementitious mortars (a) S_a and S_q, (b) S_t, S_p and S_v, (c) S_m and (d) S_{sk}, S_{ku}, S_{r1} and S_{r2}.

the scanned surface area [52,53]. Nonetheless, the kurtosis (S_{ku}) values for TiO_2 coated series were lower than (but quite close to) 3, which demonstrated a lower distribution sharpness of the tails obtained on the scanned surfaces by adding the nano-TiO_2 particles onto the surface. Comparing the area of the peak portion (S_{r1}) and the valley portion (S_{r2}) on the surface (see Fig. 5d) showed a higher area for the valleys on the scanned surface area of the reference specimen, which is in agreement with the results of the other mentioned roughness parameters. Nonetheless, by coating the surface of the specimens with nano-TiO_2 particles, the area portion of the valleys and peaks was distributed more similarly.

Finally, the surface roughness results showed a more negative surface texture for the 3D printed cementitious specimens evaluated in this study. The negative surface texture with larger space between the irregularities may have the advantage of preparing a proper substrate for applying the semiconductor particles, here nano-TiO_2. Through the existence of a large area portion for the valleys and the longer valleys depth observed for the reference specimens, there is enough area for the nano-TiO_2 particles to be deposited on the specimens' surface and thus occurring photocatalytic activity. On the other hand, the existing peaks around the valleys may add the benefits of protecting the semiconductor particles inside the valleys against the environmental conditions to guarantee an extended efficiency of the photocatalytic activity. However, the latter observation needs more in-depth study regarding the durability of the coating under distinct environmental conditions.

3.2. Photocatalytic efficiency

3.2.1. Effect of the light power intensity on the photocatalytic efficiency

Fig. 6 shows the photocatalytic efficiency of TiO_2 coated specimens with a coating rate of 20 mg/cm^2 (CR20) after 8 h of light irradiation under two different light power intensities (LPI) of 1 and 8 mW/cm^2. The photocatalytic efficiency was enhanced by increasing the higher power intensity right away from the start of the illumination process. After 8 h of illumination, series CR20 under the LPI of 8 mW/cm^2 showed about 86% higher degradation efficiency than the specimen under a LPI of 1 mW/cm^2.

The enhancement of photocatalytic efficiency considering the degradation of the organic pollutants [20,54] and NO_x removal [29] by increasing the light power intensities was also reported by other researchers. The results by Ref. [20] showed no linear relationship between degradation efficiency and radiation power intensity, which agrees with the obtained results.

3.2.2. Evaluation of the efficiency of nano-TiO_2 particles on the photocatalytic activity of the specimens

In order to assess the photocatalytic activity produced by the nano-TiO_2 particles during the tests, specimens with similar surface coating conditions were evaluated simultaneously under light exposure (L) and in the darkness (D). Two series with coating rates of 10 and 20 mg/cm^2 designated as CR10 and CR20, respectively, were chosen for evaluation. The total illumination time of 20 h was considered, while the total time under dark conditions was 24 h.

Fig. 7 shows the behaviour of specimens immersed in RhB solution under dark and light conditions. The results demonstrated a significant difference between the RhB degradation efficiency by TiO_2 coated series under light and dark conditions. Under light irradiation, the degradation efficiency resulted from the photocatalytic activity of nano-TiO_2 particles, which has started from the beginning of the illumination. The photocatalytic efficiency increased during the illumination period. The dye degradation efficiency for similar coating conditions under darkness has also increased from the initial hours of immersion in RhB solution. The degradation efficiency under darkness has occurred due to the specimens' adsorption/desorption process. Nonetheless, the degradation efficiency under darkness has reached a stationary condition after approximately 7 h.

An increase in the dye degradation efficiency of about 204% up to 486% with increasing the coating rates from 10 to 20 mg/cm^2 was observed, respectively, when comparing the corresponding series under light irradiation under darkness. This huge difference between the behaviour of TiO_2 coated series under two different conditions of illumination and darkness corroborated the extensive

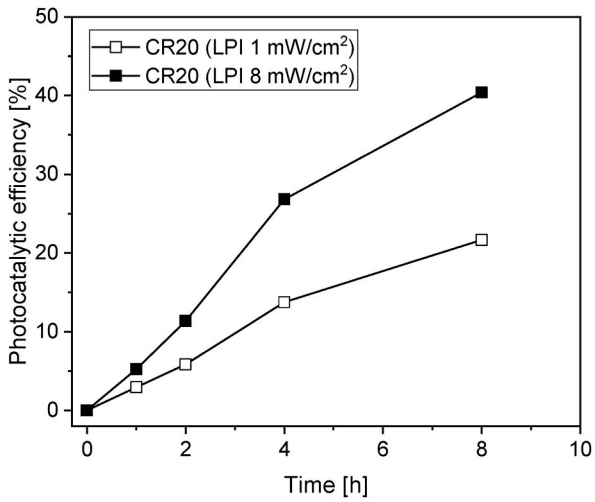

Fig. 6. The effect of light power intensity on the dye degradation efficiency.

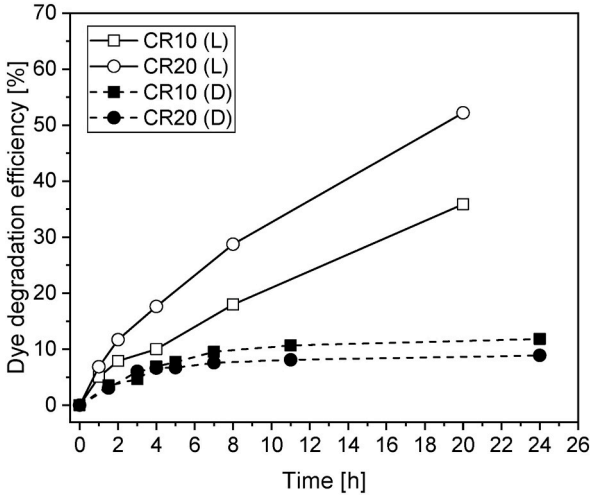

Fig. 7. Evaluation of the efficiency of nano-TiO_2 particles on the photocatalytic activity of the specimens.

photocatalytic activity of nano-TiO_2 particles under light irradiation.

3.2.3. *Effect of nano-TiO_2 coating rates on the photocatalytic efficiency*

The dye degradation efficiency of the cementitious 3D printed specimens coated with different rates of nano-TiO_2 particles was also studied. Fig. 8 shows the results of the reference specimen without coating (Ref) and the TiO_2 coated series, with coating rates of 5 (CR5), 10 (CR10), 20 (CR20), 40 (CR40) and 80 (CR80) mg/cm^2. These specimens were submitted to a light irradiation with a power intensity of 8 mW/cm^2 for 20 h, and their absorbance was measured at distinct periods, namely, 1, 2, 4, 8 and 20 h. The results showed an enhancement in the photocatalytic efficiency from the starting of the light irradiation for all the TiO_2 coated series.

The reference series (Ref) and the TiO_2 coated series of CR5 with the lowest coating rate exhibited almost a similar photocatalytic efficiency trend with a maximum difference of about 8%, which occurred for the longest illumination period, i.e., after 20 h. The series CR10 has also shown a similar photocatalytic efficiency trend to the Ref and CR5 series up to 8 h of illumination. For higher exposure time, i.e., 20 h, their photocatalytic efficiency increased up to about 32% when compared to the Ref series for the same exposure time.

The series coated with higher coating rates of nano-TiO_2 particles, such as CR20, CR40 and CR80, showed a similar trend of the photocatalytic efficiency up to 4 h of illumination. Up to 8 h of illumination, the series CR80 showed a slightly smaller photocatalytic efficiency than CR20 and CR40, respectively, about 6% and 3% lower. Nonetheless, when increasing the illumination time up to 20 h, the photocatalytic efficiency of the CR80 series has improved and had about 17% and 11% higher degradation efficiency than CR20 and CR40 series, respectively. This behaviour for the CR80 series may be ascribed to the build-up of adsorbed pollutants and the created dye decomposition products onto its surface, which could partially inactivate the reaction sites. This behaviour was also observed in the previous study by the authors [15] and also reported by Ref. [20]. Nonetheless, increasing the light exposure duration could give enough time for the decomposition products to be removed from the surface of the specimens. In this case, the nano-TiO_2

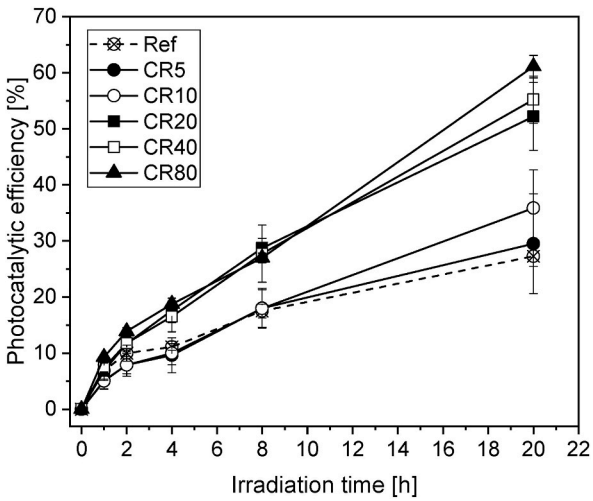

Fig. 8. Effect of TiO_2 coating rates on the photocatalytic efficiency.

particles could be reactivated again to degrade a higher quantity of pollutants. This phenomenon could be confirmed by increasing the dye degradation efficiency of the specimens at longer irradiation periods, such up to 20 h.

For all the series coated with nano-TiO_2, the maximum obtained increment on the photocatalytic efficiency value occurred with the increase of the light exposure period from 8 to 20 h, which was the longest period of light irradiation. In this case, the series CR5, CR10, CR20, CR40 and CR80 increased the photocatalytic efficiency of nearby 64%, 99%, 82%, 99% and 126%, respectively, compared with 8 h of illumination. Therefore, the results showed no constant enhancement ratio of the photocatalytic efficiency by the time of light exposure when compared to the results between the series with different coating rates. Moreover, the results showed a similar behaviour between the enhancement rates of photocatalytic efficiency for the series CR10, CR20 and CR40 when compared to series CR80. Therefore, applying a higher coating rate (i.e., 80 mg/cm^2) was necessary for this illumination period to improve the photocatalytic efficiency. This increasing trend observed on the photocatalytic efficiency between illumination periods of 8 h and 20 h contrasts with results reported by Ref. [23], in which the highest value of the photocatalytic efficiency for cement paste and mortar occurred during the first 7 h of light irradiation, followed by a constant behaviour [23].

Regarding the coating rates, results showed an increase in photocatalytic efficiency by increasing the coating rates of nano-TiO_2 particles. The minimum and the maximum photocatalytic efficiency value was obtained for the series CR5 (29.5%) and CR80 (61%), after 20 h of illumination. Between those two series, the difference on photocatalytic efficiency was around 107%. After 20 h of light irradiation, the highest increase on the photocatalytic efficiency value was about 45%, which has occurred between CR10 and CR20 series, respectively, with an efficiency of about 36% and 52%. On the other hand, the maximum difference in the photocatalytic efficiency has occurred between the series with lower coating rates, particularly for CR5 and CR10, in contrast to the series with higher coating rates, such as CR20, CR40 and CR80. Therefore, based on the obtained results, it can be concluded that higher coating rates of more than 20 mg/cm^2 did not have a significant influence on the improvement of photocatalytic behaviour, considering an increase of 6% and 17% in the photocatalytic efficiency for CR40 and CR80 series, respectively, when compared with CR20 series. The obtained results were in accordance with results reported by Refs. [19,54,55], which showed that increasing the number of TiO_2 particles may not always increase the reaction rates of photocatalytic process. Therefore, probably, there will be a threshold to the amount of semiconductor catalysts that can be applied while increasing the photocatalytic efficiency [19,54,55].

Comparing the results of the TiO_2 coated series and the reference series (Ref), it is observed an increase in dye degradation efficiency of about 8%, 32%, 91%, 102% and 124% for the series CR5, CR10, CR20, CR40 and CR80, respectively, after 20 h of illumination. After 8 h of illumination, the difference between the efficiency of TiO_2 coated series and the reference series was about 3%,

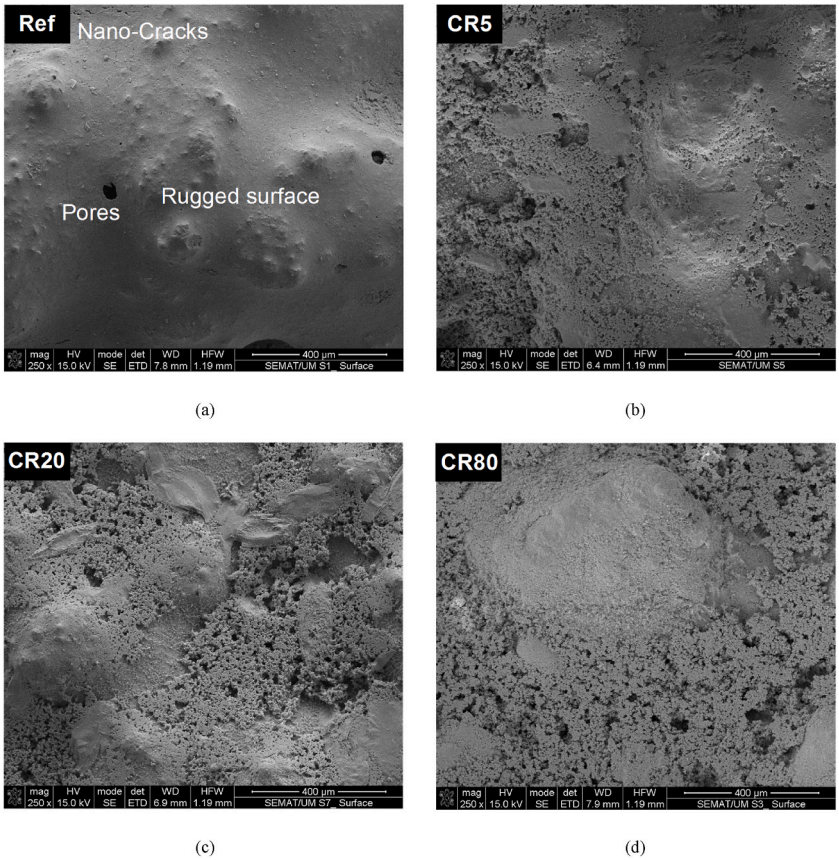

Fig. 9. SEM micrographs of the top surface of 3D printed specimens (a) Ref, (b) CR5, (c) CR20, and (d) CR80.

3%, 64%, 58%, and 54% by the series CR5, CR10, CR20, CR40, and CR80, respectively. When using higher coating rates of 20, 40 and 80 mg/cm^2, photocatalytic efficiency was even noticeable after 4 h of illumination. After 4 h of illumination, the higher photocatalytic efficiency of about 58%, 49%, and 69% was obtained for series CR20, CR40 and CR80, respectively, when compared to the reference series. To sum it up, the results showed that even low coating rates of TiO_2 could show reasonable degradation efficiencies for higher illumination periods (i.e., after 8 h), while the photocatalytic efficiency for higher coating rates was noticeable even for the shorter periods of irradiation (i.e., after 4 h).

4. Microstructural, chemical and crystallography analysis

4.1. Scanning electron microscopy

Fig. 9 shows the surface morphology of four 3D printed specimens using scanning electron microscopy (SEM). The reference (Ref) specimen showed a rugged surface with some pores and nano-cracks that can be observed on some regions on the top surface (Fig. 9a). It is worth noting that the samples prepared through 3DCP, as a freeform technology, are more prone to surface cracking due to

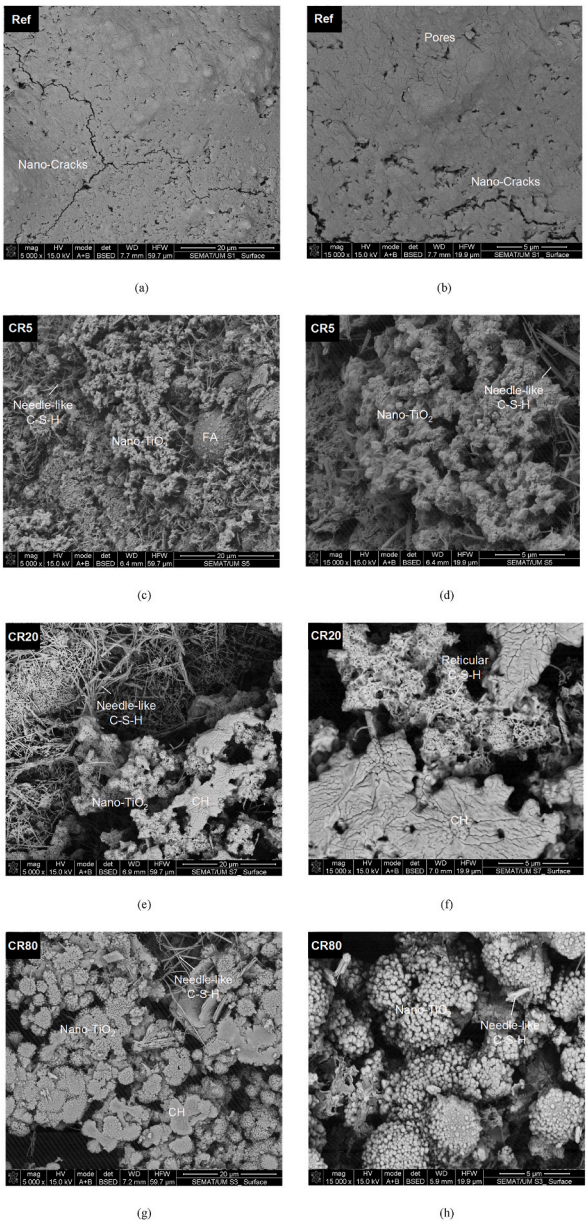

Fig. 10. SEM-BSED micrographs of the top surface of 3D printed specimens at two magnifications of 5k × ((a) Ref, (c) CR5, (e) CR20, and (g) CR80) and 15k × ((b) Ref, (d) CR5, (f) CR20, and (h) CR80).

shrinkage when compared to the mould cast specimens [56]. On the other hand, the surface morphology of the TiO_2 coated series (Fig. 9b, c, and d) were quite different compared to the Ref specimen. The formation and existence of numerous aggregates were quite clear on the surface of TiO_2 coated series. Covering the surface by the formed aggregates resulted in a reduction in the surface's ruggedness. Therefore, a less rugged surface morphology can be observed on the top surface of TiO_2 coated series when compared to the Ref specimen. Indeed, the rugged surface of the Ref specimen acted as a proper area for the formation and settling down the new aggregates (i.e., here the nano-TiO_2 particles). This observation agrees with the results of the surface roughness micro-analysis (see Section 3.1).

Fig. 10 shows the SEM micrographs, using a back-scattered electron detector (BSED), of the specimens in two different magnifications of 5k × and 15k × . The specimens' surfaces showed clear differences between Ref and TiO_2 coated series (CR5, CR20 and CR80). On the surface of TiO_2 coated series, regardless of the coating rates, the existence of nano-TiO_2 particles was observed. It can be observed that nano-TiO_2 particles are distributed on the surface of the specimens on top or among the other compounds resulting from the hydration process of cementitious materials. The presence of needle-like and reticular forms of calcium silicate hydrate (C–S–H) and calcium hydroxide ($Ca(OH)_2$) as two main hydration products of cementitious materials was detected on the surface.

Moreover, unlike the TiO_2 coated specimens, the hydration products could not be observed on the surface of the Ref series (Fig. 10a and b). This could occur due to covering the surface of the uncoated specimens by a thin film that prevented the hydration product from being visible under SEM analysis. Nonetheless, the air pressure during the coating process could change the coated series' surface morphology resulting in the appearance of hydration products in addition to nano-TiO_2 particles (Fig. 10c, d, e, f, g, and h).

4.2. *Energy-dispersive X-ray spectroscopy*

Fig. 11 shows the results of EDS spectrums of the top surfaces of the 3D printed specimens. The EDS results were used to compare the chemical elemental compositions on the surface of Ref and TiO_2 coated (CR5, CR20, and CR80) series. The EDS spectrum clearly showed the existence of nano-TiO_2 on the surface of the TiO_2 coated series regardless of the coating rates. These results confirmed the observations from SEM-BSED micrographs based on the chemical elemental compositions. As previously mentioned, in Sec 3.3.1, the nano-TiO_2 particles are scattered on the surface among other typical hydration products of cementitious materials. Therefore, the elemental spectrum showed also the existence of the calcium (Ca) and silicate (Si) as two major chemical elements on the top surface of all the specimens (i.e., Ref and TiO_2 coated series). Moreover, the results showed an extensive reduction of silicate on the surface of the TiO_2 coated series by increasing the coating rates (i.e. CR20 and CR80 series). Increasing the nano-TiO_2 coating rates could cover the silicate that was already detected in the higher amounts on top of the surface of Ref and CR5 series.

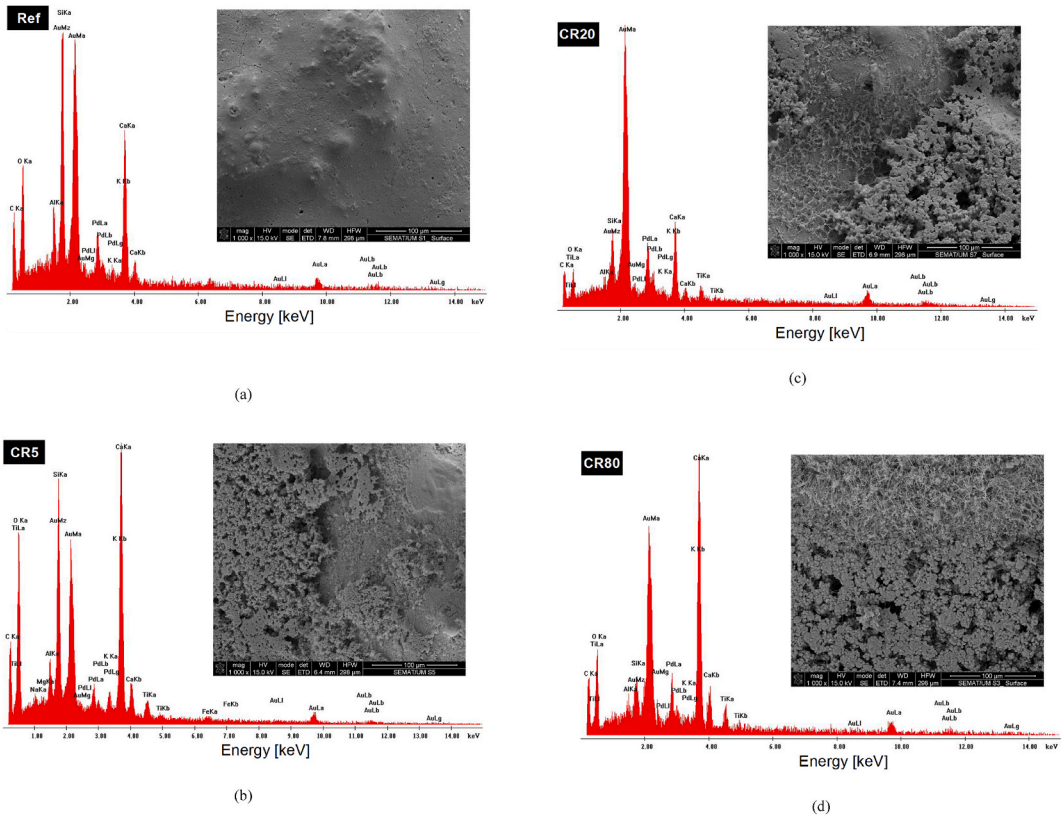

Fig. 11. SEM-EDS analysis at the top surface of 3D printed specimens of (a) Ref, (b) CR5, (c) CR20, and (d) CR80.

Fig. 12 shows the comparison between the amount of titanium element in its oxide form (i.e., TiO_2) distributed on the surface of the coated specimens. As expected, the highest (10.2 wt%) and the lowest (3.35 wt%) content of nano-TiO_2 particles were detected on the surfaces of series CR80 and CR5, respectively. The series CR20 with 8.86 wt% of distributed nano-TiO_2 particles on its surface showed a 13% lower amount of nano-TiO_2 when compared to series CR80. This relatively small difference between the distribution of nano-TiO_2 particles on the surface of the series CR20 and CR80 agrees with the results of dye degradation efficiency of these series (See Sec. 3.2.3). In spite of the coating rate of CR80 being 4 times higher than the one from CR20, the difference between the amount of distributed nano-TiO_2 particles on the surface, as well the dye degradation efficiency was not significantly different. Agglomeration of the nano-TiO_2 particles or removal of the particles excess from the top surface due to the saturation phenomena can be two potential reasons for the observed results for the coating rates higher than CR20.

In order to evaluate the dispersion of the nano-TiO_2 particles on the surface of the coated series, two random zones (Z1 and Z2) on the surface of series CR80 were selected for EDS analysis. Fig. 13 shows the SEM micrograph and related EDS spectrums for Z1 and Z2 of series CR80. The SEM micrograph and the chemical elemental analysis both showed that the nano-TiO_2 particles were concentrated more in Z2 (7.51 wt%) when compared to Z1 (1.99 wt%). In the Z1, the nano-TiO_2 particles were less exposed as they are partially covered by the cementitious hydration products, mainly needle-like C–S–H. However, in Z2, the nano-TiO_2 particles were more exposed, so the EDS analysis showed a higher concentration on the elemental spectrum.

A cross section perpendicular to the nano-TiO_2 coated surface was also evaluated through SEM micrographs and related EDS analysis. The main reason for performing these analyses on this cross section cut was to evaluate the potential in-depth penetration of the nano-TiO_2 particles near their coated surface. It should be reminded that the specimens were coated by the nano-TiO_2 particles immediately after the printing process when the cementitious mortar was still fresh (See Sec. 2.2) and the hydration process of the cement was undergoing. Fig. 14 shows the SEM micrographs and related EDS spectrums on the selected cross section of series CR80. The Z'1 (bulk zone) shows an area with a maximum depth of 40 μm (Fig. 14a), while the Z'2 (zone nearer the coating surface) shows an area with a maximum depth of 2 μm (Fig. 14b) from the top surface of the CR80 series. The EDS chemical elemental analysis showed the existence of nano-TiO_2 particles in both areas of Z'1 and Z'2.

The concentration of nano-TiO_2 particles was about 112% higher at Z'2 (6.67 wt%) when compared to Z'1 (3.15 wt%). The results showed that the nano-TiO_2 particles partially penetrated the specimens, while most of their concentration was near the specimens' surface at a depth of 2 μm. The latter can indicate that an adequate immobilization process occurred for nano-TiO_2 particles on the surface of the coated series. The penetration of the nano-TiO_2 particles underneath the coating surface may benefit from exposing the particles after any potential surface abrasion/wear under real-life environmental conditions. In this case, the penetrated nano-TiO_2 particles can be exposed during life-span of the coated element and continue their photocatalytic efficiency through reactivation under light irradiation. Nonetheless, a more in-depth study about the durability of the nano-TiO_2 coated specimens is required to confirm the continuous photocatalytic efficiency over time under environmental conditions.

4.3. X-ray diffraction crystallography

X-ray diffraction crystallography, XRD, analysis was carried out on Ref and CR80 series on both top surface and cross section. Fig. 15 shows the results of the XRD analysis. It can be observed that almost the same minerals resulting from cement hydration process have been observed, on both sides of the specimens. The abundant minerals were quartz (Q), calcite (C), portlandite (P), and tobermorite (T) for both series of Ref and CR80. Furthermore, only on the top surface of the series $CR80_{(TOP)}$, the presence of nano-TiO_2 particles was also detected beyond the hydration products. The nano-TiO_2 anatase crystalline phase can be confirmed by the presence of some diffraction peaks such as (101) and (220) crystallographic planes appearing at the angular positions of $2\theta \cong 26.5^\circ$ and $2\theta \cong 70.1^\circ$, respectively. On the other hand, the diffraction peaks (101) and (200) detected at the angular positions of $2\theta \cong 35.6^\circ$ and $2\theta \cong$

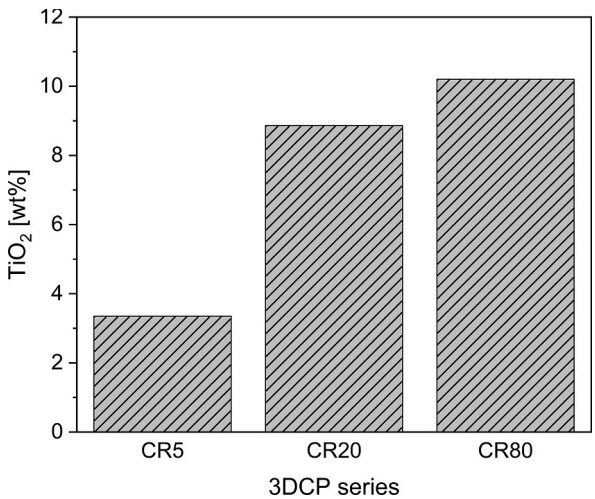

Fig. 12. Distribution amount of the nano-TiO_2 particles on the surface of the TiO_2 coated specimens resulting from EDS analysis.

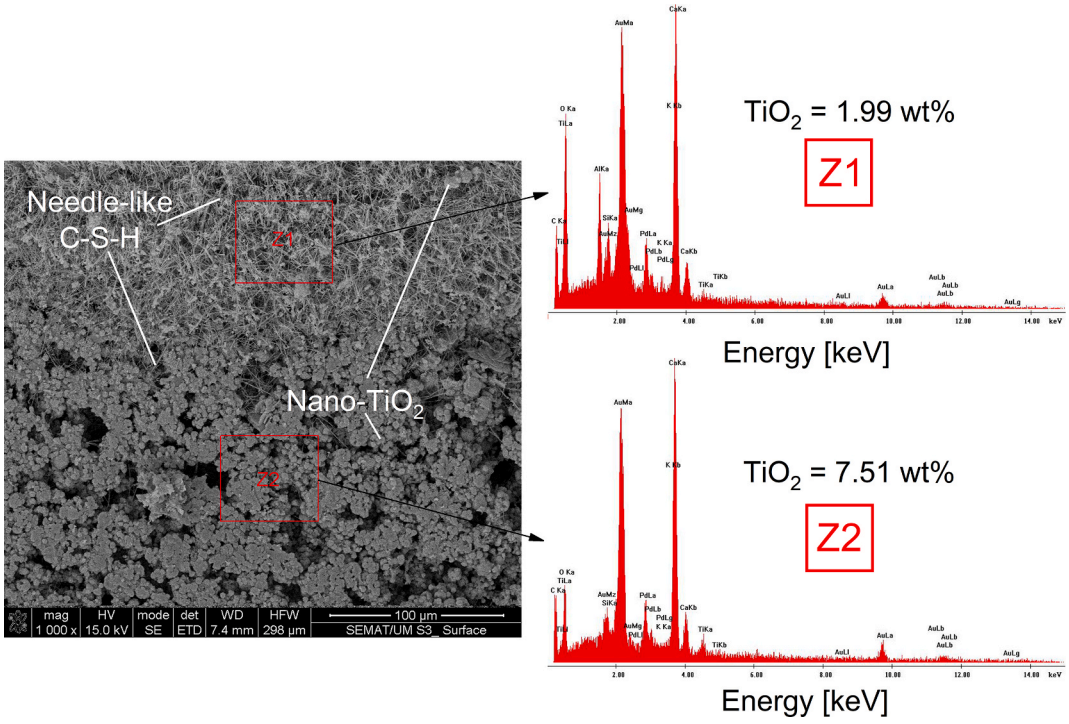

Fig. 13. SEM-EDS analysis on the top surfaces of series CR80 at Z1 and Z2.

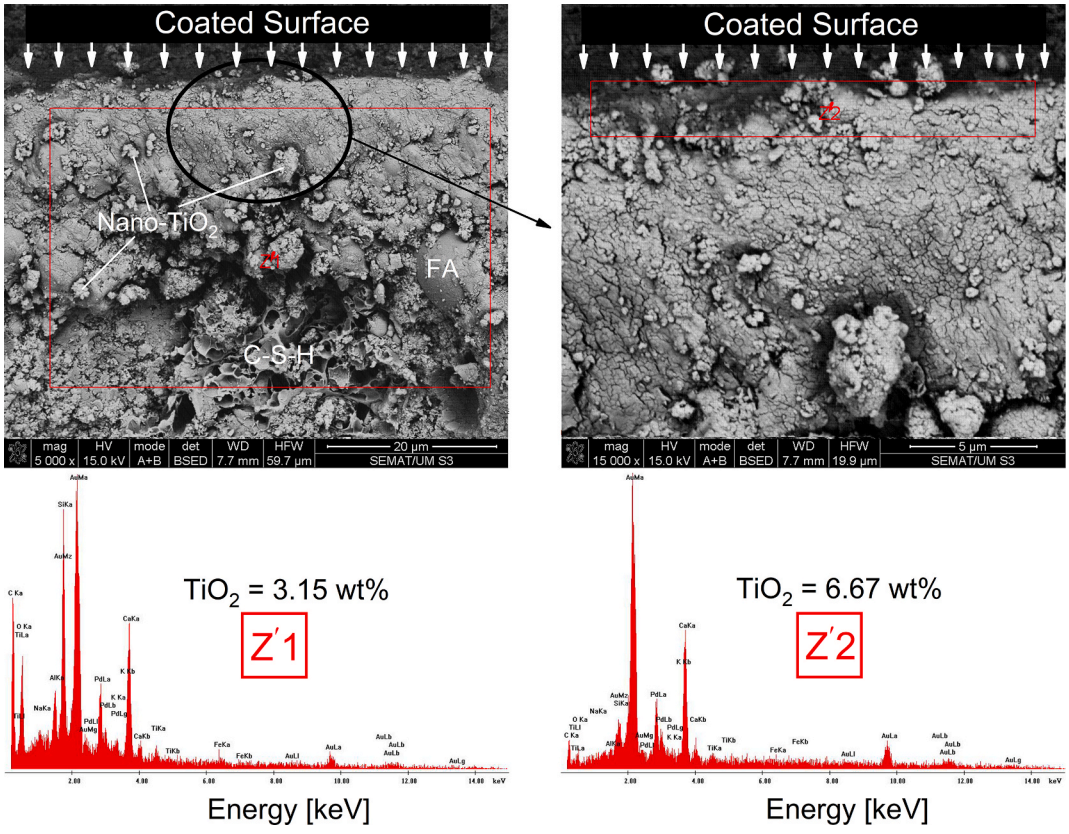

Fig. 14. SEM-EDS analysis on the cross section of series CR80 at (a) Z'1 and (b) Z' 2.

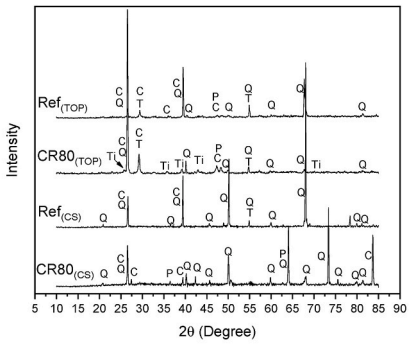

Q: Quartz; C: Calcite; P: Portlandite; T: Tobermorite; Ti: TiO_2; TOP: Top Surface; CS: Cross Section

Fig. 15. XRD analysis of series Ref and CR80 on the top surface and cross section of the specimens.

39.5°, respectively, are associated with the presence of the nano-TiO_2 rutile crystalline phase. The Scherrer's equation [35,57] was employed to determine the mean grain size of the TiO_2 nanoparticles. The obtained values (calculated from the full width at the half maximum intensity of the mentioned peaks of each crystalline phase) were about 22 nm and 28 nm for the anatase and rutile phase, respectively. These results are similar to those obtained in previous works [35,48]. Moreover, the results of XRD analysis are also in agreement with the results obtained from observations of SEM micrographs and the chemical elemental analysis using the EDS characterisation technique.

5. Conclusions

In this study, the photocatalytic behaviour of 3D printed mortars focused on the RhB dye degradation efficiency was evaluated. Moreover, the roughness surface texture and the microstructure of this smart material were also evaluated in order to allow a more comprehensive analysis of the photocatalytic behaviour. The coating application procedure to achieve photocatalytic properties was combined with 3DCP technology to develop a functionalised material, which has the potential to be fully automated based on advanced manufacturing techniques. The main results of this study can be summarised as follow.

- The surface analysis of the 3D printed specimens showed a negative surface texture for the specimens with large spaces between the irregularities that could make their surfaces suitable for depositing the semiconductor particles.
- The photocatalytic efficiency was enhanced 86% by increasing the light power intensity from 1 to 8 mW/cm^2 during 8 h of illumination.
- Comparing the photocatalytic efficiency of the specimens with the same surface coating condition under two different situations of illumination and darkness showed the extensive photocatalytic activity of the nano-TiO_2 particles under light irradiation. The CR10 and CR20 series (10 and 20 mg/cm^2 of spray ratio of nano-TiO_2, respectively) showed an increase of 204% up to 486% in photocatalytic activity up to 20 h of illumination when compared to the same series under darkness.
- Specimens with various nano-TiO_2 coating rates showed enhancement of dye degradation efficiency by increasing the coating rates up to 124% for series CR80 (80 mg/cm^2 of spray ratio of nano-TiO_2) when compare to Ref series (without nano-TiO_2) after 20 h of illumination. Even though the increasing of coating rates showed an enhancement in photocatalytic efficiency, but the maximum efficient amount of the nano-TiO_2 particles should be considered. The results showed 6% and 17% of enhancement in photocatalytic efficiency of CR40 (40 mg/cm^2 of spray ratio of nano-TiO_2) and CR80 series when compare to CR20 series.
- Different microstructure analyses (SEM, EDS and XRD) revealed the existence of the nano-TiO_2 particles on the surface of the coated specimens, which was in agreement with the results obtained from photocatalytic activity. The morphology of the specimen's surfaces could also confirm the observations from surface roughness micro-analysis.
- The CR80 sample (80 mg/cm^2 of nano-TiO_2 aqueous solution) presented the highest photocatalytic efficiency, which had the best distribution of TiO_2 nanoparticles at the coated surface.

The use of smart materials in construction is gaining momentum, and the combination of 3D printing and photocatalysis in cementitious mortars represents a promising new combination of two novel techniques. By developing this smart material for the construction sector, may endow the built environment to degrade harmful gases such as SO_x and NO_x, as well as adsorb organic compounds, leading to cleaner air and an improved aesthetic of buildings and infrastructure. Additionally, the incorporation of 3D printing into the manufacturing process of the cementitious mortar enables greater flexibility in design and construction, resulting in structures with unique geometries and tailored properties. Besides, these capabilities can be feasibly integrated since it is not necessary any mould cast, allowing the application of TiO_2 nanoparticles immediately after the printing and, consequently, improving their immobilization on the cementitious mortar.

This novel approach to materials engineering not only provides solutions for environmental pollution, but it also offers a promising new direction for the development of smart materials with enhanced capabilities. The application of photocatalysis and 3D printing in cementitious mortars opens up new avenues for the construction industry, with the potential to create more efficient and sustainable structures. As such, this exciting area of research has the potential to transform the field of civil engineering, and pave the way for more

environmentally conscious construction practices in the future.

The incorporation of nanomaterials into the Architecture, Engineering and Construction (AEC) sector presents an opportunity for the nanotechnology industry since it will handle the employment of large-scale of nanomaterials. The suppliers of nanomaterials can capitalize on this opportunity due to the market scale of the AEC sector and develop new products that meet the unique needs and specifications of the construction industry, dynamizing this market.

Funding

This work was partly financed by Fundação para a Ciência e a Tecnologia (FCT)/MCTES through national funds (PIDDAC) under the R&D Unit Institute for Sustainability and Innovation in Structural Engineering (ISISE), under reference UIDB/04029/2020. The authors acknowledge the support of DST group construction company for funding the project Chair dst/IB-S: Smart Systems for Construction. The first two authors would like to acknowledge the PhD grants SFRH/BD/143636/2019 and SFRH/BD/137421/2018 provided by the Portuguese Foundation for Science and Technology (FCT). Additionally, the authors would like to acknowledge FCT for the financing this research work by the project NanoAir PTDC/FIS-MAC/6606/2020 and the Strategic Funding UIDB/04650/2020–2023.

Author statement

Behzad Zahabizadeh: Conceptualisation, Methodology, Formal Analysis, Investigation, Writing-Original Draft Preparation, Writing-Review and Editing. **Iran Rocha Segundo:** Conceptualisation, Methodology, Formal Analysis, Investigation, Writing-Original Draft Preparation, Writing-Review and Editing **João Pereira:** Writing-Review and Editing. **Elisabete Freitas:** Methodology, Writing-Review and Editing. **Aires Camões:** Writing-Review and Editing. **Vasco Teixeira:** Writing-Review and Editing. **Manuel F. M. Costa:** Writing-Review and Editing. **Vítor M.C.F. Cunha:** Conceptualisation, Methodology, Investigation, Writing-Review and Editing, Supervision. **Joaquim O. Carneiro:** Conceptualisation, Methodology, Investigation, Writing-Review and Editing, Supervision. All authors have read and agreed to the published version of the manuscript.

Declaration of competing interest

The authors declare that they have no known competing financial interests or personal relationships that could have appeared to influence the work reported in this paper.

Data availability

Data will be made available on request.

Acknowledgements

The authors appreciate the support SECIL, SIKA, ELKEM and UNIBETAO, which graciously provided the required materials for printing the cementitious specimens.

References

[1] G. Hüsken, M. Hunger, H.J.H. Brouwers, Experimental study of photocatalytic concrete products for air purification, Build. Environ. 44 (2009) 2463–2474, https://doi.org/10.1016/j.buildenv.2009.04.010.
[2] J.V.S. de Melo, G. Trichês, Evaluation of the influence of environmental conditions on the efficiency of photocatalytic coatings in the degradation of nitrogen oxides (NOx), Build, Environ. Times 49 (2012) 117–123, https://doi.org/10.1016/j.buildenv.2011.09.016.
[3] C. Mendoza, A. Valle, M. Castellote, A. Bahamonde, M. Faraldos, TiO2 and TiO2–SiO2 coated cement: comparison of mechanic and photocatalytic properties, Appl. Catal. B Environ. 178 (2015) 155–164, https://doi.org/10.1016/j.apcatb.2014.09.079.
[4] M.M. Ballari, Q.L. Yu, H.J.H. Brouwers, Experimental study of the NO and NO2 degradation by photocatalytically active concrete, Catal. Today 161 (2011) 175–180, https://doi.org/10.1016/j.cattod.2010.09.028.
[5] S. Kim, J. Seo, H.N. Yoon, H.K. Lee, Exploration of effects of CO2 exposure on the NOx-removal performance of TiO2-incorporated Portland cement evaluated via microstructural and morphological investigation, J. Build. Eng. 45 (2022), 103609, https://doi.org/10.1016/j.jobe.2021.103609.
[6] P. Sikora, K. Cendrowski, A. Markowska-Szczupak, E. Horszczaruk, E. Mijowska, The effects of silica/titania nanocomposite on the mechanical and bactericidal properties of cement mortars, Construct. Build. Mater. 150 (2017) 738–746, https://doi.org/10.1016/j.conbuildmat.2017.06.054.
[7] I. Rocha Segundo, C. Ferreira, E.F. Freitas, J.O. Carneiro, F. Fernandes, S.L. Júnior, M.F. Costa, Assessment of photocatalytic, superhydrophobic and self-cleaning properties on hot mix asphalts coated with TiO2 and/or ZnO aqueous solutions, Construct. Build. Mater. 166 (2018) 500–509, https://doi.org/10.1016/j.conbuildmat.2018.01.106.
[8] C. Chen, B. Tang, X. Cao, F. Gu, W. Huang, Enhanced photocatalytic decomposition of NO on portland cement concrete pavement using nano-TiO2 suspension, Construct. Build. Mater. 275 (2021), 122135, https://doi.org/10.1016/j.conbuildmat.2020.122135.
[9] M.V. Diamanti, B. Del Curto, M. Ormellese, M.P. Pedeferri, Photocatalytic and self-cleaning activity of colored mortars containing TiO2, Construct. Build. Mater. 46 (2013) 167–174, https://doi.org/10.1016/j.conbuildmat.2013.04.038.
[10] M. Smits, D. Huygh, B. Craeye, S. Lenaerts, Effect of process parameters on the photocatalytic soot degradation on self-cleaning cementitious materials, Catal. Today 230 (2014) 250–255, https://doi.org/10.1016/j.cattod.2013.10.001.
[11] A. Ajmal, I. Majeed, R.N. Malik, H. Idriss, M.A. Nadeem, Principles and mechanisms of photocatalytic dye degradation on TiO $_2$ based photocatalysts: a comparative overview, RSC Adv. 4 (2014) 37003–37026, https://doi.org/10.1039/C4RA06658H.
[12] Segundo Rocha, Landi Freitas Jr., Carneiro Costa, Smart, photocatalytic and self-cleaning asphalt mixtures: a literature review, Coatings 9 (2019) 696, https://doi.org/10.3390/coatings9110696.
[13] J.O. Carneiro, S. Azevedo, V. Teixeira, F. Fernandes, E. Freitas, H. Silva, J. Oliveira, Development of photocatalytic asphalt mixtures by the deposition and volumetric incorporation of TiO2 nanoparticles, Construct. Build. Mater. 38 (2013) 594–601, https://doi.org/10.1016/j.conbuildmat.2012.09.005.

[14] L. Zou, Y. Luo, M. Hooper, E. Hu, Removal of VOCs by photocatalysis process using adsorption enhanced TiO2–SiO2 catalyst, Chem. Eng. Process. Process Intensif. 45 (2006) 959–964, https://doi.org/10.1016/j.cep.2006.01.014.

[15] B. Zahabizadeh, I.R. Segundo, J. Pereira, E. Freitas, A. Camões, C.J. Tavares, V. Teixeira, V.M.C.F. Cunha, M.F.M. Costa, J.O. Carneiro, Development of photocatalytic 3D-printed cementitious mortars: influence of the curing, spraying time gaps and TiO2 coating rates, Buildings 11 (2021) 381, https://doi.org/10.3390/buildings11090381.

[16] A. Fujishima, X. Zhang, D. Tryk, TiO2 photocatalysis and related surface phenomena, Surf. Sci. Rep. 63 (2008) 515–582, https://doi.org/10.1016/j.surfrep.2008.10.001.

[17] S. Shen, M. Burton, B. Jobson, L. Haselbach, Pervious concrete with titanium dioxide as a photocatalyst compound for a greener urban road environment, Construct. Build. Mater. 35 (2012) 874–883, https://doi.org/10.1016/j.conbuildmat.2012.04.097.

[18] M.-Z. Guo, T.-C. Ling, C.-S. Poon, Nano-TiO2-based architectural mortar for NO removal and bacteria inactivation: influence of coating and weathering conditions, Cem. Concr. Compos. 36 (2013) 101–108, https://doi.org/10.1016/j.cemconcomp.2012.08.006.

[19] S. Feng, J. Song, F. Liu, X. Fu, H. Guo, J. Zhu, Q. Zeng, X. Peng, X. Wang, Y. Ouyang, F. Li, Photocatalytic properties, mechanical strength and durability of TiO2/cement composites prepared by a spraying method for removal of organic pollutants, Chemosphere 254 (2020), 126813, https://doi.org/10.1016/j.chemosphere.2020.126813.

[20] A. Enesca, L. Isac, The influence of light irradiation on the photocatalytic degradation of organic pollutants, Materials 13 (2020) 2494, https://doi.org/10.3390/ma13112494.

[21] A.M. Ramirez, N. De Belie, Application of TiO2 photocatalysis to cementitious materials for self-cleaning purposes, in: Y. Ohama, D. Van Gemert (Eds.), Appl. Titan. Dioxide Photocatal. Constr. Mater., Springer Netherlands, Dordrecht, 2011, pp. 11–15, https://doi.org/10.1007/978-94-007-1297-3_3.

[22] F. Hamidi, F. Aslani, TiO2-based photocatalytic cementitious composites: materials, properties, influential parameters, and assessment techniques, Nanomaterials 9 (2019) 1444, https://doi.org/10.3390/nano9101444.

[23] B. Ruot, A. Plassais, F. Olive, L. Guillot, L. Bonafous, TiO2-containing cement pastes and mortars: measurements of the photocatalytic efficiency using a rhodamine B-based colourimetric test, Sol. Energy 83 (2009) 1794–1801, https://doi.org/10.1016/j.solener.2009.05.017.

[24] A.M. Ramirez, K. Demeestere, N. De Belie, T. Mäntylä, E. Levänen, Titanium dioxide coated cementitious materials for air purifying purposes: preparation, characterisation and toluene removal potential, Build. Environ. 45 (2010) 832–838, https://doi.org/10.1016/j.buildenv.2009.09.003.

[25] J. Chen, S. Kou, C. Poon, Photocatalytic cement-based materials: comparison of nitrogen oxides and toluene removal potentials and evaluation of self-cleaning performance, Build, Environ. Times 46 (2011) 1827–1833, https://doi.org/10.1016/j.buildenv.2011.03.004.

[26] E. Jimenez-Relinque, J.R. Rodriguez-Garcia, A. Castillo, M. Castellote, Characteristics and efficiency of photocatalytic cementitious materials: type of binder, roughness and microstructure, Cement Concr. Res. 71 (2015) 124–131, https://doi.org/10.1016/j.cemconres.2015.02.003.

[27] S.S. Lucas, V.M. Ferreira, J.L.B. de Aguiar, Incorporation of titanium dioxide nanoparticles in mortars — influence of microstructure in the hardened state properties and photocatalytic activity, Cement Concr. Res. 43 (2013) 112–120, https://doi.org/10.1016/j.cemconres.2012.09.007.

[28] A. Folli, C. Pade, T.B. Hansen, T. De Marco, D.E. Macphee, TiO2 photocatalysis in cementitious systems: insights into self-cleaning and depollution chemistry, Cement Concr. Res. 42 (2012) 539–548, https://doi.org/10.1016/j.cemconres.2011.12.001.

[29] M.-Z. Guo, T.-C. Ling, C.S. Poon, Photocatalytic NO x degradation of concrete surface layers intermixed and spray-coated with nano-TiO 2 : influence of experimental factors, Cem. Concr. Compos. 83 (2017) 279–289, https://doi.org/10.1016/j.cemconcomp.2017.07.022.

[30] Y. Bao, M. Xu, D. Soltan, T. Xia, A. Shih, H.L. Clack, V.C. Li, Three-dimensional printing multifunctional engineered cementitious composites (ECC) for structural elements, in: T. Wangler, R.J. Flatt (Eds.), First RILEM Int. Conf. Concr. Digit. Fabr. – Digit. Concr. 2018, Springer International Publishing, Cham, 2019, pp. 115–128, https://doi.org/10.1007/978-3-319-99519-9_11.

[31] T. Nochaiya, W. Wongkeo, A. Chaipanich, Utilisation of fly ash with silica fume and properties of Portland cement–fly ash–silica fume concrete, Fuel 89 (2010) 768–774, https://doi.org/10.1016/j.fuel.2009.10.003.

[32] V.M.C.F. Cunha, PhD thesis, in: Steel Fibre Reinforced Self-Compacting Concrete (From Micromechanics to Composite Behavior), vol. 331, University of Minho, Guimarães, Portugal, 2010.

[33] B. Zahabizadeh, J. Pereira, C. Gonçalves, E.N.B. Pereira, V.M.C.F. Cunha, Influence of the printing direction and age on the mechanical properties of 3D printed concrete, Mater. Struct. 54 (2021) 73, https://doi.org/10.1617/s11527-021-01660-7.

[34] B. Zahabizadeh, J. Pereira, C. Gonçalves, V.M.C.F. Cunha, Development of cement-based mortars for 3D printing through wet extrusion, in: IABSE Symp. 2019 Guimarães Resilient Built Environ. - Risk Asset Manag., 2019. Guimarães, Portugal.

[35] J.O. Carneiro, S. Azevedo, F. Fernandes, E. Freitas, M. Pereira, C.J. Tavares, S. Lanceros-Méndez, V. Teixeira, Synthesis of iron-doped TiO2 nanoparticles by ball-milling process: the influence of process parameters on the structural, optical, magnetic, and photocatalytic properties, J. Mater. Sci. 49 (2014) 7476–7488, https://doi.org/10.1007/s10853-014-8453-3.

[36] I.G. da Rocha Segundo, S. Landi Jr., S.M.B. Oliveira, E.F. de Freitas, J.A.O. Carneiro, Photocatalytic asphalt mixtures: mechanical performance and impacts of traffic and weathering abrasion on photocatalytic efficiency, Catal. Today 326 (2019) 94–100, https://doi.org/10.1016/j.cattod.2018.07.012.

[37] I. Rocha Segundo, S. Landi Jr., S. Oliveira, E. Freitas, M.F. Costa, J. Carneiro, Photocatalytic asphalt mixtures: semiconductors' impact in skid resistance and texture, Road Mater. Pavement Des. 20 (2019) S578–S589, https://doi.org/10.1080/14680629.2019.1624398.

[38] M.V. Diamanti, M. Ormellese, M. Pedeferri, Characterisation of photocatalytic and superhydrophilic properties of mortars containing titanium dioxide, Cement Concr. Res. 38 (2008) 1349–1353, https://doi.org/10.1016/j.cemconres.2008.07.003.

[39] M. Faraldos, R. Kropp, M.A. Anderson, K. Sobolev, Photocatalytic hydrophobic concrete coatings to combat air pollution, Catal. Today 259 (2015) 228–236, https://doi.org/10.1016/j.cattod.2015.07.025.

[40] T. Meng, Y. Yu, X. Qian, S. Zhan, K. Qian, Effect of nano-TiO2 on the mechanical properties of cement mortar, Construct. Build. Mater. 29 (2012) 241–245, https://doi.org/10.1016/j.conbuildmat.2011.10.047.

[41] J. Chen, S. Kou, C. Poon, Hydration and properties of nano-TiO2 blended cement composites, Cem. Concr. Compos. 34 (2012) 642–649, https://doi.org/10.1016/j.cemconcomp.2012.02.009.

[42] M.F.M. Costa, V. Teixeira, Rugometric and microtopographic inspection of Cr–Cr $_2$ O $_3$ cermet solar absorbers, Int. J. Photoenergy. 2007 (2007) 1–6, https://doi.org/10.1155/2007/82327.

[43] M.F.M. Costa, Optical triangulation-based microtopographic inspection of surfaces, Sensors 12 (2012) 4399–4420, https://doi.org/10.3390/s120404399.

[44] ISO 4287, Geometrical Product Specifications (GPS) — Surface Texture: Profile Method — Terms, Definitions and Surface Texture Parameters, 1997.

[45] ISO 21920-2, Geometrical Product Specifications (GPS) — Surface Texture: Profile — Part 2: Terms, Definitions and Surface Texture Parameters, 2021.

[46] D. Whitehouse, Profile and areal (3D) parameter characterisation, in: Surf. Their Meas, vol. 1, publ, HPS, London, 2002, pp. 48–95.

[47] W. Shen, C. Zhang, Q. Li, W. Zhang, L. Cao, J. Ye, Preparation of titanium dioxide nano particle modified photocatalytic self-cleaning concrete, J. Clean. Prod. 87 (2015) 762–765, https://doi.org/10.1016/j.jclepro.2014.10.014.

[48] S. Landi, J.O. Carneiro, F. Fernandes, P. Parpot, J. Molina, F. Cases, J. Fernández, J.G. Santos, G.M.B. Soares, V. Teixeira, A.P. Samantilleke, Functionalization of cotton by RGO/TiO2 to enhance photodegradation of rhodamine B under simulated solar irradiation, water, Air. Soil Pollut. 228 (2017) 335, https://doi.org/10.1007/s11270-017-3533-z.

[49] N. Barka, S. Qourzal, A. Assabbane, A. Nounah, Y. Ait-Ichou, Factors influencing the photocatalytic degradation of Rhodamine B by TiO2-coated non-woven paper, J. Photochem. Photobiol. Chem. 195 (2008) 346–351, https://doi.org/10.1016/j.jphotochem.2007.10.022.

[50] H. Lachheb, E. Puzenat, A. Houas, M. Ksibi, E. Elaloui, C. Guillard, J.-M. Herrmann, Photocatalytic degradation of various types of dyes (alizarin S, crocein orange G, methyl red, Congo red, methylene blue) in water by UV-irradiated titania, Appl. Catal. B Environ. 39 (2002) 75–90, https://doi.org/10.1016/S0926-3373(02)00078-4.

[51] P.M.D. Santos, E.N.B.S. Júlio, A state-of-the-art review on roughness quantification methods for concrete surfaces, Construct. Build. Mater. 38 (2013) 912–923, https://doi.org/10.1016/j.conbuildmat.2012.09.045.

[52] N. Duboust, H. Ghadbeigi, C. Pinna, S. Ayvar-Soberanis, A. Collis, R. Scaife, K. Kerrigan, An optical method for measuring surface roughness of machined carbon fibre-reinforced plastic composites, J. Compos. Mater. 51 (2017) 289–302, https://doi.org/10.1177/0021998316644849.
[53] G. Shamsutdinova, M.A.N. Hendriks, S. Jacobsen, Topography studies of concrete abraded with ice, Wear 430–431 (2019) 1–11, https://doi.org/10.1016/j.wear.2019.04.017.
[54] Q. Wang, K. Zheng, H. Yu, L. Zhao, X. Zhu, J. Zhang, Laboratory experiment on the nano-TiO_2 photocatalytic degradation effect of road surface oil pollution, Nanotechnol. Rev. 9 (2020) 922–933, https://doi.org/10.1515/ntrev-2020-0072.
[55] L. Yang, F. Wang, C. Shu, P. Liu, W. Zhang, S. Hu, TiO2/porous cementitious composites: influences of porosities and TiO2 loading levels on photocatalytic degradation of gaseous benzene, Construct. Build. Mater. 150 (2017) 774–780, https://doi.org/10.1016/j.conbuildmat.2017.06.004.
[56] G.M. Moelich, J. Kruger, R. Combrinck, Plastic shrinkage cracking in 3D printed concrete, Compos. B Eng. 200 (2020), 108313, https://doi.org/10.1016/j.compositesb.2020.108313.
[57] R. Jenkins, R.L. Snyder, Introduction to X-Ray Powder Diffractometry, 1., Auflage, John Wiley & Sons, New York, NY, 2012.